Entry length requirements for direct simulations of turbulent boundary layers

By J. Jiménez, M. P. Simens, S. Hoyas AND Y. Mizuno†

1. Motivation and objectives

This report describes the results of a relatively large-scale direct simulation of a turbulent boundary layer using a new simulation code, with emphasis on the extent of the contamination of the flowfield due to the inflow boundary conditions. The assumption is that the goal of the simulation is to explore the physics of the flow, about which it is desirable to make as few assumptions as possible. Conclusions for cases in which turbulence itself is not the primary concern may differ from the present ones. The flow geometry is kept simple; a parallelepiped over a flat wall, with an upper boundary far enough into the freestream to model flow at infinity. Transpiration velocities over that boundary can be manipulated to create arbitrary pressure distributions, and they are chosen to keep the pressure gradient as low as possible.

Turbulent boundary layers have been subjects of interest from the first days of fluid mechanics, especially the canonical case with zero pressure gradient. As a consequence, they were some of the first flows to be simulated (Spalart 1988; Spalart & Watmuff 1993), but the Reynolds numbers of those simulations have increased more slowly than for streamwise-homogeneous flows, such as in the channels (Kim *et al.* 1987; Hoyas & Jiménez 2006). Part of the reason is that boundary layers are harder to compute because they are inhomogeneous in at least two directions, but equally important is that they require inflow boundary conditions. In transitional cases this is relatively straightforward because the inflow is laminar, but even there the question of how to seed the perturbations has to be considered. Transition in boundary layers is typically subcritical, and its details depend on the level and character of the upstream perturbations. That is why experiments are usually tripped, and why some equivalent mechanism is needed in simulations. If the problem of transition is to be completely avoided, some way has to be devised to generate a turbulent inflow, and this non-trivial question has been the subject of a lot of work.

Although the boundary layer is a spatially developing flow, attempts have often been made to reintroduce periodicity in the numerical problem, in some cases to retain spectral methods, and in others to use the outflow as a convenient source of realistic fluctuations to synthesize a turbulent inflow. The strategies that use spectral methods further subdivide into those in which the flow is expanded in terms of a slow growth plus periodic small-scale fluctuations (Spalart 1988, 1986), and those in which the outflow is damped to minimize the spectral errors due to edge discontinuities, and reintroduced at the inflow after some manipulation (Spalart & Watmuff 1993). Although Nordström *et al.* (1999) have shown that those "fringe" methods are accurate, and although they have been used to simulate boundary layers at relatively high Reynolds numbers (Alam & Sandham 2000; Skote & Henningson 2002; Khurajadze & Oberlack 2004), one of the effects of the damping is that the incoming flow is typically almost laminar, and that increasing the

† School of Aeronautics, Universidad Politécnica, 28040 Madrid, Spain

Reynolds numbers becomes expensive. A further problem is that periodicity is difficult to reconcile with strong spatial inhomogeneity, such as strong pressure gradients, or with control strategies involving net mass injection.

Once spectral accuracy is abandoned, the choice of inflow strategies becomes wider, and reduces to determining how a synthetic turbulent inflow can be made to converge fastest to a more realistic structure. A recent survey by Keat *et al.* (2004), although primarily concerned with large-eddy simulations and therefore with low-order statistics, shows that it is difficult to create inflows with accommodation lengths shorter than several boundary layer thicknesses. In the present paper we use the version of the fringe method introduced by Lund *et al.* (1998) in which an intermediate flow plane is rescaled and copied to the inflow without damping. Our primary interest is to determine how much of the simulation domain has to be discarded before the flow can be assumed to have forgotten the artificial inflow.

The structure of the paper is as follows. The basic code is introduced in Sect. 2. The boundary layer simulation is briefly described in Sect. 3, and a more detailed discussion of the effect of the turbulent inflow procedure is presented in Sect. 3.1. A preliminary report on some of the material presented here is Simens (2008), which also contains examples of application of the code to other problems. Further implementation details can be found in Simens *et al.* (2009).

2. Problem formulation

The code uses a relatively classical fractional-step method, such as described by Kim & Moin (1985); Dukowicz & Dvinsky (1992); Perot (1993), to solve the Navier–Stokes equations expressed in primitive variables. Adaptations to improve resolution and efficiency include fourth-order compact finite differences for the advective terms in the streamwise and wall-normal directions, but only second-order operators for the pressure. It is shown by Simens *et al.* (2009) that this combination reduces the accuracy of the code, but not its resolution.

The components of the velocity vector $\mathbf{u}$ are u, v and w in the streamwise, x, wall-normal, y, and spanwise, z, directions. The boundary conditions at the inflow and at the top and bottom $(x-z)$ planes depend on the flow being simulated, but the domain is always periodic in the z direction. The velocities at the outflow are estimated by a convective boundary condition,

$$\partial_t \mathbf{u} + U_c \partial_x \mathbf{u} \approx 0, \tag{2.1}$$

where U_c is usually the freestream velocity at the exit, with small corrections to enforce global mass conservation.

The fractional-step method is implemented in terms of an approximate LU decomposition of the semi-discrete primitive-variable operator, as explained in Perot (1993), and time stepping is by the semi-implicit three-step Runge–Kutta described in Spalart *et al.* (1991). The nonlinear and wall-parallel viscous terms are treated explicitly. The linear implicit part includes only the viscous terms in the y-direction. It was shown by Akselvoll & Moin (1996) that this does not lead to excessively small time steps in pipes, and we have found the same in boundary layers.

The convective and viscous terms in the x and y directions are calculated using staggered three-point compact finite differences (Nagarajan *et al.* 2003), while the velocity and pressure are expanded in Fourier series along z. No staggering is used in that direc-

Re_θ	$(L_x, L_y, L_z)/\theta$	$\Delta x^+, \Delta y^+, \Delta z^+$	$\Delta y/\eta$	N_x, N_y, N_z
600-950	$210 \times 41 \times 43$	$6.7 \times 0.70 \times 4.6$	1.2	$1282 \times 258 \times 386$
620–2140	$535 \times 29 \times 88$	$6.1 \times 0.30 \times 4.1$	1.4	$6145 \times 360 \times 1536$

TABLE 1. Parameters of the boundary layer simulations. L_x, L_y and L_z are the box dimensions along the three axes. N_x, N_y and N_z are the corresponding grid sizes, expressed for z in terms of collocation points, and the Δ's are the resolutions, given at their coarsest points. The values in the top line are representative of the several short-box test simulations (SB), and those at the bottom belong to the production run (LB). The Kolmogorov length η is computed from the local energy dissipation. The coarsest resolution along x and z in terms of η is found at the wall, where $\eta^+ \approx 1.5$. The resolution given in the table for y is reached at $y \approx \delta_{99}/2$, where $\eta^+ \approx 3$. The reference momentum thickness, θ, is taken at the center of the simulation box.

tion, and the computation of the non-linear terms is pseudo-spectral, using the 2/3 rule to prevent aliasing.

The time step is adjusted to a constant CFL. Although the time stepper is stable up to $CFL \approx 1.7$, the simulations described below are run with $CFL \approx 0.5 - 1$ to preserve time accuracy.

3. The turbulent boundary layer simulation

The code is used to simulate a turbulent zero-pressure-gradient boundary layer, with the turbulent inflow generated by the recycling scheme of Lund *et al.* (1998).

Both in that reference, where the inflow was used to drive a large-eddy simulation, and in later direct simulations by Ferrante & Elgobashi (2004), the method is typically applied by running a smaller spatially periodic simulation from which the inflow plane is extracted to the main inflow. If both the auxiliary and the main simulations belong to the same flow, we find little reason to separate them, and here we use a downstream plane of the main simulation, x_{ref}, as a reference from which to synthesize the inflow.

Lund's method is known to be delicate to apply (Ferrante & Elgobashi 2004; Liu & Pletcher 2006), and Sect. 3.1 will be devoted to our experience with it. Before that, we summarize the results of the two sets of simulations performed. Their parameters are given in Table 1. The "short" simulation SB is representative of a family of tests used to tune the numerical scheme, whose numerical parameters, such as box height or grid resolution, were varied by factors of up to two from those given in the table. Typical grids for these cases are in the range of 100 Mpoints.

Simulation LB was intended as a production run. It is one of the highest-Reynolds-number boundary layer simulations presently available, and its results from the point of view of fluid dynamics will be discussed in future papers. Here we restrict ourselves to numerical issues. The average streamwise pressure gradient is controlled by applying a constant uniform suction at the upper boundary, which is otherwise stress-free. The transpiration velocity is estimated from the known experimental growth of the displacement thickness, δ^*, in that range of Reynolds numbers. This keeps the acceleration coefficient $\beta = \delta^* U_\infty^+ \partial_x U_\infty^+$ to $\beta \approx 2 \times 10^{-4}$, which is reasonably small, but the gradient increases sharply to $\beta \approx 5 \times 10^{-3}$ within the last 5% of the numerical domain. This corresponds to the last 1.5 boundary layer thicknesses, and is clearly due to the effect of the outflow,

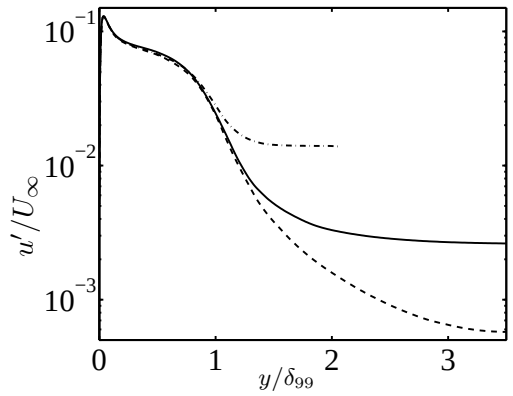

FIGURE 1. Fluctuations of the streamwise velocity for three simulations with different box heights. $Re_\theta = 930$. —·— , SB, $L_y/\delta_{99e} = 1.75$; ——— , LB, $L_y/\delta_{99e} = 2.4$; - - - - , SB, $L_y/\delta_{99e} = 3.6$.

which uses no numerical sponge in this particular case. That region is discarded from the results.

The intensity of the freestream velocity fluctuations (Fig. 1) turns out to be controlled by the ratio between the height of the computational box and the boundary layer thickness at the exit, δ_{99e} , and remains almost constant with x. The freestream velocity fluctuations for the LB run are about $2.5 \times 10^{-3} U_\infty$, and the corresponding vorticity fluctuations are about $2 \times 10^{-3} U_\infty/\delta_{99e}$. They are also roughly independent of x, rather than scaling with the local δ_{99}. That scaling and constancy suggest that the residual freestream fluctuations consist mostly of large-scale vorticity waves advected by the free stream, and introduced at the inflow by the sloshing created by the interaction of the boundary layer with the exit. Such fluctuations are unavoidable. The streamwise derivatives $\partial_x v$ and $\partial_x w$ cannot be imposed at the inflow boundary, and there is no way of enforcing the strict irrotationality of the inflow. The incoming vorticity is fixed by the global pressure fluctuations, which are in turn created when the largest eddies leave the domain. The resulting vorticity fluctuations are weak, but because they have sizes comparable to those of the large outgoing eddies, they are not damped by viscosity, and cross the simulation domain essentially undisturbed.

Figure 2(a) shows the development of the friction coefficients of the two simulations, given in the form $U_\infty^+ = (2/C_f)^{1/2}$ †, as functions of the Reynolds number, $Re_\theta = U_\infty \theta/\nu$. They are compared with the simulations of Spalart (1988), and with the experimental results of Erm & Joubert (1991), which cover roughly the same range of Reynolds numbers. The latter experiments are particularly interesting because they were designed to test the effect of the tripping, which is probably comparable to the effect of the numerical inflow. All their measurements were repeated with three different tripping devices, which are plotted in Fig. 2 using different symbols. The result was that the effect of the trip survives up to $Re_\theta \approx 1500$, and only becomes small beyond that limit. It is seen in Fig. 2(a) that the same is true in our results, which initially diverge widely from the experiments, but eventually settle into excellent agreement with them at about the same location at which the experimental scatter begins to decrease.

Figures 2(b, c) present mean and fluctuation streamwise velocities roughly at the cen-

† Wall-scaled variables are defined in terms of the local friction velocity $u_\tau(x)$ and of the molecular viscosity ν, and denoted by a + superindex.

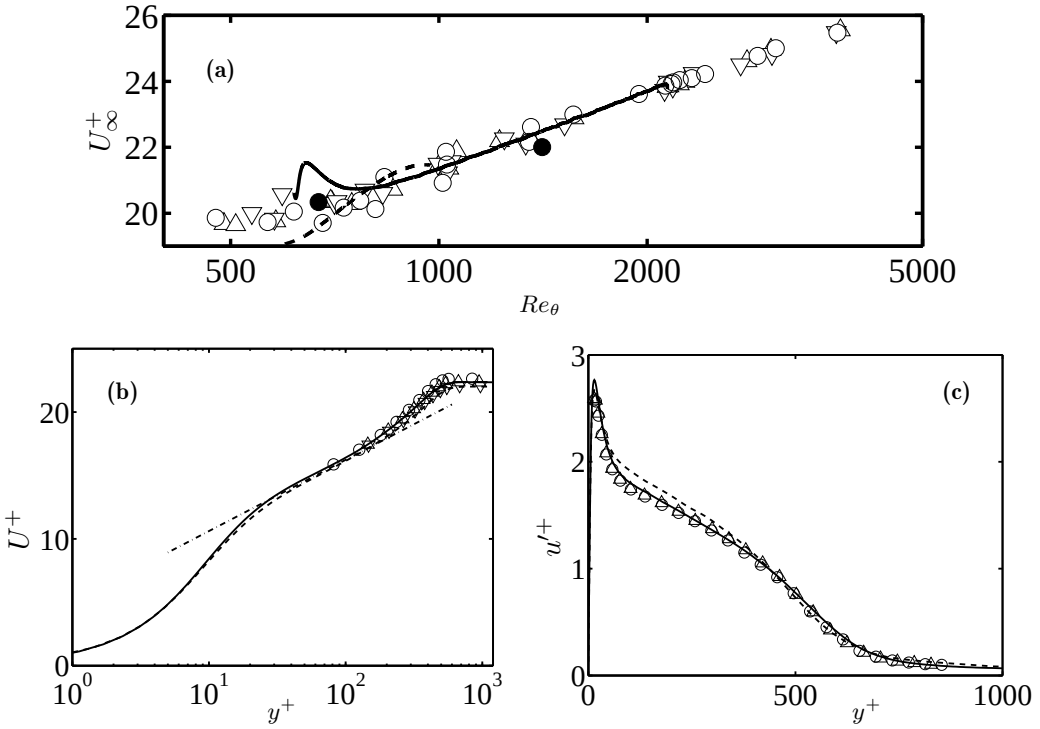

FIGURE 2. (a) Friction coefficient versus Reynolds number. Open symbols are experiments from Erm & Joubert (1991), tripped by △ , wire; ▽ , grit; ○ , pins; • , simulations in Spalart (1988). ——— , LB simulation; - - - - , representative SB simulation. (b) Mean streamwise velocity. ——— , LB simulation at $Re_\theta = 1350$; - - - - , simulation in Spalart (1988), $Re_\theta = 1410$. Open symbols are as in (a), with $Re_\theta \approx 1350$. —·— , $\log(y^+)/0.41 + 5$. (c) Root-mean-squared streamwise velocity. Symbols as in (b), but $Re_\theta \approx 1550$, both for Erm & Joubert (1991) and for LB.

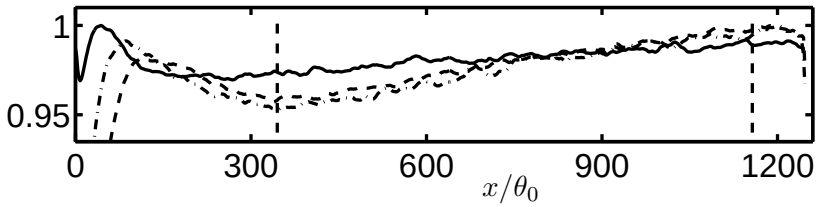

FIGURE 3. Peak value of the three velocity-fluctuation intensities, normalized to a common level for the purpose of plotting. Simulation LB. ——— , u'/u_τ; - - - - , v'/u_τ; —·— , w'/u_τ. The dashed vertical lines are the limits of the "useful" range.

ter of the computational domain of LB, together with the closest available experimental Reynolds numbers. The agreement is excellent in both cases. The older simulation by Spalart (1988) at a roughly similar Reynolds number is also included. The minor discrepancies of those fluctuations with both the present results and with the experiments cannot be attributed to the Reynolds number difference, and are probably due to the mean-flow expansion used to approximate the flow.

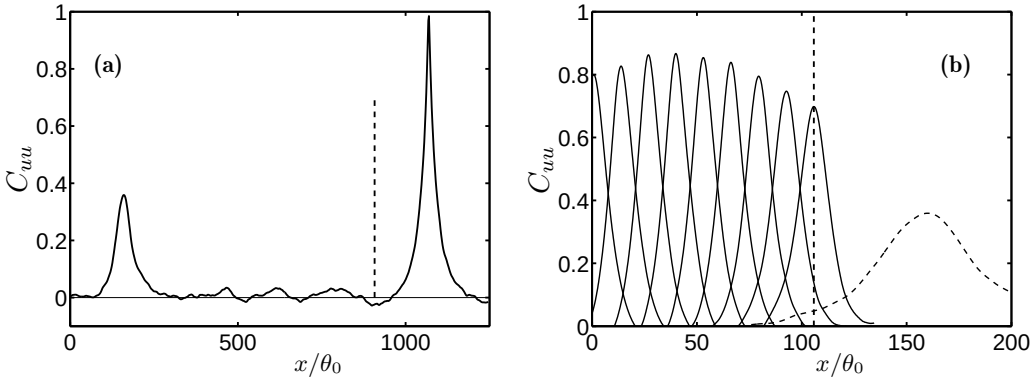

FIGURE 4. (a) Correlation $C_{uu}(x;x')$ of the streamwise velocity in simulation LB, as a function of x. (b) Secondary peaks of C_{uu}, for various values of x'. ——— , SB; - - - - , LB. For both simulations the correlation is only computed for a band of spanwise wavenumbers $\lambda_z/\delta_{99,ref} = (1.2 - 2.3)$, at $y/\delta_{99,ref} \approx 0.4$. The dashed vertical line in (a) is the location of the inflow reference plane for LB. The one in (b) is for SB.

3.1. *The effect of the inflow*

Most of the adjustments required by our code for this particular application were connected with the turbulent inflow condition. This was not due to the incorrect performance of the recycling method itself, which was applied much as described in the original publication by Lund *et al.* (1998). For example, Ferrante & Elgobashi (2004) reported problems initializing simulations from random data, and proposed solutions. Our simulations were initialized from a filtered field from Spalart (1988), and extended gradually, and did not require any such modification.

The problem seems to arise from the dynamics of the flow itself, and is probably common to most methods of generating synthetic inflows. It is clear from Fig. 2(a) that a substantial initial part of the box has to be discarded. The evolution of flow properties that reside farther from the wall than the friction coefficient actually suggests that the problem affects the first 25% of the box (Fig. 3). This, together with the shorter segment contaminated by the outflow, means that about one-third of the box has to be discarded, and that the range of useful Reynolds numbers is reduced from the values in Table 1 to about $Re_\theta = 1100 - 2050$.

The reason for the long inflow length can be seen in Fig. 4(a), which displays the autocorrelation function $C_{uu}(x;x')$ of a band of spanwise Fourier coefficients of the streamwise velocity, as a function of x. Besides the primary peak at $x = x' \approx 1100\theta_0$, there is a secondary peak at $x = x' - x_{ref} \approx 150\theta_0$. Lund's method can be interpreted as a physical experiment in which eddies at the reference plane are approximately (except for rescaling) copied to a different position in the boundary layer (the inflow), and evolved. The correlation between the reference and the inflow planes is always large, because one is almost a copy of the other. When the correlation is computed with respect to some location downstream of the reference plane, it reflects, besides the local structure of the eddies, the correspondence between eddies that have been advected from the reference and from the inflow planes. This is the origin of the secondary peak in Fig. 4(a), and its decay with $x' - x_{ref}$ is a measure of the Lagrangian decorrelation time of the eddies as they are advected by the mean velocity. Both the range of spanwise wavenumbers in Fig. 4, and the y location of the correlations, have been chosen to maximize the amplitude

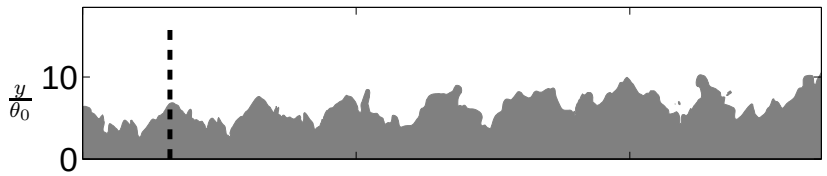

FIGURE 5. Streamwise $(x - y)$ section of an SB simulation in which the inflow reference plane is at $x_{ref}/\theta_0 = 32$, represented by the dashed vertical line. The gray area is $U < 0.9U_\infty$. Note the spurious periodic structures.

of the secondary peak. It is interesting that they correspond to spanwise wavelengths of the order of $\lambda_z/\delta_{99,ref} \approx 1.5$, which is somewhat wider than, but of the same order as, the large-scale structures identified in this region of experimental boundary layers by Tomkins & Adrian (2005).

The decay of the secondary peak as it moves away from the inflow is shown in Fig. 4(b), and is exceedingly slow. The peaks from the short simulation, in which the reference plane is close to the inflow, have decayed very little by the time they reach x_{ref}. A secondary peak from the LB simulation, in which $x_{ref}/\theta_0 = 850$, and for which the correlation of the inflow with the reference plane is presumably lower than in SB because of the larger rescaling ratio, is still clearly visible at $x/\theta_0 \approx 160$. It has been known for a long time that the decay of the space-time velocity correlation in boundary layers is much slower when the two points are at "optimum" separations than when they are at the same location, showing that the eddies stay coherent while being advected for much longer distances than their lengths. For example, Favre *et al.* (1958) found that, while the correlation length of u was only a few δ_{99}, the correlation along the optimum advection speed had only decayed to about 0.8 after $4\delta_{99}$ ($\approx 35\theta$). Figure 4(b) suggests that eddies would stay coherent for $200 - 300\theta$, which is consistent with the lengths found for the persistence of the tripping influence in Erm & Joubert (1991). The physical reason for this long inflow length is that the turnover time for a large eddy of size $O(\delta)$, with internal velocities $O(u_\tau)$, is δ/u_τ, during which time the eddy is advected by about $U_\infty\delta/u_\tau$. The implied accommodation lengths, of order $U_\infty^+\delta$, are consistent with the values found above.

Note that the actual persistence of the eddies is probably about twice longer than what can be deduced from Fig. 4(b), because the inflow 'experiment' tests the decorrelation of two eddies as they diverge from each other, while a single eddy probably decorrelates with itself about twice slower. Note also that the apparent growth of the correlation at intermediate locations of Fig. 4(b) is due to the correlation being computed at a constant y, while the optimum correlation is known to occur between eddies at similar values of y/δ_{99} (Favre *et al.* 1958).

The practical consequence from the point of view of numerical inflow conditions is that the first few hundred momentum thicknesses of a boundary layer are controlled by the inflow, and that they cannot therefore be used to investigate the structure of turbulence. Better inflow fields may be useful to create more realistic flows, which could for example be used to investigate the effects of turbulence on some other aspect of the flow, but when the physics of the turbulence itself is what is being investigated, the first few hundred momentum thicknesses essentially reflect the hypotheses made for the inflow conditions. Note that this is a problem of any inflow, not only of the recycling method, and that the inflow length estimated here would have to be added to any other length contaminated by local numerical manipulations (e.g., fringes).

In the case of Lund's method, the eddy persistence can give rise to numerical artifacts

if the reference plane is chosen too close to the inlet. An example is shown in Fig. 5, which corresponds to an early SB simulation in which $x_{ref}/\theta_0 = 32$. The inflow couples to the reference plane, creating an artificial periodicity that can be seen even in instantaneous velocity maps. Doubling the reference distance to $x_{ref}/\theta_0 = 60$ decreases the effect, although it is still visible in the correlations. No periodicity can be detected in the LB simulation, where $x_{ref}/\theta_0 = 850$.

When the inflow coupling is added to other numerical problems, the effect can be even more marked. In another SB test, with a reference plane close to the inflow and a low upper boundary, the coupling became strong enough to create periodic vorticity "chimneys" extending across the whole height of the box, raising the freestream turbulence level to $O(1)$. Similar effects in a pipe were reported in Nikitin (2007).

4. Discussion

We have presented a new numerical code for boundary layer simulations that can be used with and without pressure gradients, and with arbitrary time-dependent velocity boundary conditions. It uses a fractional-step primitive-variable formulation with fourth-order compact finite differences on a staggered grid for the convective and viscous terms, and a standard second-order scheme for the divergence of the velocity and for the gradient of the pressure.

The code is used for a relatively large-scale simulation of a turbulent zero-pressure-gradient boundary layer with a useful range of $Re_\theta \approx 1100 - 2050$, within which the agreement with experimental results is excellent.

The turbulent inflow is synthesized using Lund *et al.* (1998) recycling method. It is found that the first several hundred momentum thicknesses have to be discarded because they retain the effect of the synthetic inflow. It is argued that this is a property of the flow itself, similar to the persistence of tripping effects, and not of the particular inflow scheme. Together with a shorter contaminated segment at the outflow, it amounts to approximately one-third of our longest simulation box, and spans the full extent of the shorter boxes used for code tuning. A similar fraction was mentioned for the fringe method by Spalart & Watmuff (1993), but the present limit is not connected with the numerical manipulation of the affected region, and our results suggest that both lengths would have to be added in cases in which part of the flow is locally contaminated by the numerics.

The same eddy persistence responsible for the inflow length implies that the reference plane used to synthesize the incoming turbulence should be as far as possible from the inflow, or at least farther than $20 - 30$ boundary layer thicknesses. Otherwise the two planes tend to couple, creating spurious flow periodicities that, in extreme cases, may result in large freestream oscillations, or even in numerical divergence. An obvious constraint is that the plane used as reference should not be within the part of the flow corrupted by the exit condition. A less obvious one is that the rescaling ratio increases with the distance from the reference to the inflow, so that the incoming turbulence becomes less realistic as that distance is increased. The value chosen for the present simulation, $x_{ref} = 850\theta_0 \approx 90\delta_{99,0}$ is probably close to the largest practical one.

Acknowledgments

This work was supported in part by the Advanced Simulation and Computing program of the Department of Energy, by grant TRA2006-08226 of the Spanish CICYT, and by the

EU FP6 Wallturb Strep AST4-CT-2005-516008. The computations were made possible by generous grants of computer time from the Barcelona Supercomputing Center, and by the equally generous collaboration of the Port d'Informació Científica (PIC), which lent their mass storage facilities to archive raw data. MPS was supported in part by the EU FP5 Training and Mobility Network HPRN-CT-2002-00300, and SH and YM by the Spanish Ministry of Education and Science, under the Juan de la Cierva program.

The author is grateful to Oscar Flores for his careful critique of an earlier version of this manuscript.

REFERENCES

Akselvoll, K. & Moin, P. 1996 An efficient method for temporal integration of the Navier-Stokes equations in confined axisymmetric geometries. *J. Comp. Phys.* **125**, 454–463.

Alam, M. & Sandham, N. D. 2000 Direct numerical simulation of short laminar separation bubbles with turbulent reattachment. *J. Fluid Mech.* **410**, 1–28.

Dukowicz, J. K. & Dvinsky, A. S. 1992 Approximate factorization as a high order splitting for the implicit incompressible flow equations. *J. Comp. Phys.* **102**, 336–347.

Erm, L. P. & Joubert, P. N. 1991 Low-Reynolds-number turbulent boundary layers. *J. Fluid Mech.* **230**, 1–44.

Favre, A. J., Gaviglio, J. J. & Dumas, R. J. 1958 Further space-time correlations of velocity in a turbulent boundary layer. *J. Fluid Mech.* **3**, 344–356.

Ferrante, A. & Elgobashi, S. E. 2004 A robust method for generating inflow conditions for direct simulations of spatially-developing turbulent boundary layers. *J. Comp. Phys.* **198**, 372–387.

Hoyas, S. & Jiménez, J. 2006 Scaling of the velocity fluctuations in turbulent channels up to $Re_\tau = 2003$. *Phys. Fluids* **18**, 011702.

Keat, A., Piomelli, U., Ballaras, E. & Kaltenbach, H. 2004 A priori and a posteriori tests of inflow conditions for large-eddy simulations. *Phys. Fluids* **16**, 4696–4712.

Khurajadze, G. & Oberlack, M. 2004 DNS and scaling laws from new symmetry groups of ZPG turbulent boundary layer flow. *Theor. Comp. Fluid Dyn.* **18**, 391–441.

Kim, J. & Moin, P. 1985 Application of a fractional-step method to incompressible Navier-Stokes equations. *J. Comp. Phys.* **59**, 308–323.

Kim, J., Moin, P. & Moser, R. D. 1987 Turbulence statistics in fully developed channel flow at low Reynolds number. *J. Fluid Mech.* **177**, 133–166.

Liu, K. & Pletcher, R. H. 2006 Inflow conditions for the large-eddy simulation of turbulent boundary layers: A dynamic procedure. *J. Comp. Phys.* **219**, 1–6.

Lund, T. S., Wu, X. & Squires, K. D. 1998 Generation of turbulent inflow data for spatially-developing boundary layer simulations. *J. Comp. Phys.* **140**, 233–258.

Nagarajan, S., Lele, S. K. & Ferziger, J. H. 2003 A robust high-order compact method for large eddy simulation. *J. Comp. Phys.* **191**, 329–419.

Nikitin, N. 2007 Spatial periodicity of spatially evolving turbulent flow caused by inflow boundary condition. *Phys. Fluids* **19**, 091703.

Nordström, J., Nordin, N. & Henningson, D. 1999 The fringe region technique and the Fourier method used in the direct numerical simulation of spatially evolving viscous flows. *SIAM J. Sci. Comput.* **90**, 1365–1393.

Perot, J. B. 1993 An analysis of the fractional step method. *J. Comp. Phys.* **108**, 51–58.

Simens, M. P. 2008 The study and control of wall-bounded flows. PhD thesis, Aeronautics, U. Polit. Madrid, http://oa.upm.es/1047/.

Simens, M. P., Jiménez, J., Hoyas, S. & Mizuno, Y. 2009 A high-resolution code for turbulent boundary layers. *J. Comp. Phys.* Submitted.

Skote, M. & Henningson, D. S. 2002 Direct numerical simulation of a separated turbulent boundary layer. *J. Fluid Mech.* **471**, 107–136.

Spalart, P. R. 1986 Numerical study of sink-flow boundary layers. *J. Fluid Mech.* **172**, 307–328.

Spalart, P. R. 1988 Direct simulation of a turbulent boundary layer up to $Re_\theta = 1410$. *J. Fluid Mech.* **187**, 61–98.

Spalart, P. R., Moser, R. D. & Rogers, M. M. 1991 Spectral method for the Navier–Stokes equations with one infinite and two periodic dimensions. *J. Comput. Phys.* **96**, 297–324.

Spalart, P. R. & Watmuff, J. H. 1993 Experimental and numerical study of a turbulent boundary layer with pressure gradients. *J. Fluid Mech.* **249**, 337–371.

Tomkins, C. D. & Adrian, R. J. 2005 Energetic spanwise modes in the logarithmic layer of a turbulent boundary layer. *J. Fluid Mech.* **545**, 141–162.